Available online at www.sciencedirect.com
SCIENCE DIRECT®
ELSEVIER
European Journal of Mechanics B/Fluids 21 (2002) 721–738
EUROPEAN JOURNAL OF MECHANICS B/FLUIDS

On the variation of 'spot' properties with pressure gradient

Susan N. Brown *, Frank T. Smith

Department of Mathematics, University College London, Gower Street, London WC1E 6BT, UK

Received 11 April 2001; accepted 15 August 2002

Abstract

The evolution of a linear disturbance in a laminar boundary layer is described by the three-dimensional Euler equations. The basic profile is piecewise linear, and is chosen to model favourable and unfavourable pressure gradients as the pressure-gradient parameter, B, increases. Earlier investigation for the case $B = 0$ showed that, at large values of the time, the algebraically-decaying oscillatory perturbation is confined to a horizontally-expanding region of the boundary layer. The phenomenon is interpreted as, or resembles, an incipient turbulent spot.

The main contribution of the present work is an investigation of the effect of B. There are two quite different outcomes as $|B|$ increases. On the favourable ($B < 0$) side the spot splits into two. The parts at first overlap but then move in tandem downstream through the boundary layer. The oscillatory perturbation is confined to their interiors. On the adverse ($B > 0$) side the spot splits into two non-overlapping regions separated by a region in which the disturbance increases exponentially with time. As B increases still further, the trailing edge of the spot starts to move upstream and the instability is now absolute. Some comparisons are made, in particular of spot-spread angle, with existing experiments under favourable and adverse pressure gradients.

Keywords: Stability; Pressure gradients; Spots

1. Introduction

A prominent feature of turbulent flows such as those in turbo-machinery is the occurrence of spot concentrations of disturbances in the boundary layer. Experimentally, these are observed to grow with time and often to have a distinctive arrowhead shape with a calmed trailing-edge region. Practical data of interest include leading and trailing-edge speeds and spot-spreading angle, in addition to the distribution of the disturbance throughout the various regions of the spot. Many of the earlier experiments, for example, Schubauer and Klebanoff [1], Wygnanski et al. [2], Sankaran et al. [3], Katz et al. [4], were for zero or favourable pressure gradient flows. The effects of adverse pressure gradients were studied by Gostelow et al. [5], Seifert and Wygnanski [6] and van Hest et al. [7], and in Gostelow et al. [8], and D'Ovidio et al. [9,10] the authors studied the turbulent development of basic flows near and beyond the conditions of laminar separation. The relatively large loading on compressor and turbine blades tends to produce extensive zones of flow under adverse pressure gradient.

These turbulent flows are complex and are seldom amenable to analytical study. In order to gain some insight into the development of such disturbance concentrations it has been found worthwhile to examine an analogous phenomenon in laminar flow. In such a scenario it is anticipated that laminar spots, especially if unstable with growing perturbations, are a feature of a boundary layer immediately prior to transition (and may also indicate broad characteristics of turbulent spots). There are then various possibilities for such an investigation. Is it sufficient for the three-dimensional stability analysis to be linear and for non-parallel effects to be ignored? Should the effects of an adverse pressure gradient be accommodated and is compressibility

* Corresponding author.
E-mail address: snb@math.ucl.ac.uk (S.N. Brown).

0997-7546/02/$ – see front matter
PII: S0997-7546(02)01206-2

important? An early paper which built on the concept of a spot as the result of the long-time development of an initial disturbance is that of Doorly and Smith [11]. There a non-linear inviscid model is set-up, but is analysed as an initial-value problem after linearisation. The long-time disturbances are decaying waves confined to a wedge in the boundary layer bounded by a caustic. Strictly, the pressure gradient may be adverse, but is not sufficiently large to affect the spot development at leading order. The caustic itself, in the neighbourhood of which the perturbations are largest, was studied as were the effects of Mach number; the predicted spreading-angle dependence on Mach number agrees with the later experimental findings of Clark et al. [12]. In a subsequent paper, Bowles and Smith [13], hereinafter referenced as BS, the authors showed that a linear profile with a slope discontinuity led to closure of the inviscid spot at both leading and trailing edges, and bore qualitative and some quantitative comparison to the experiments. In the long wavelength limit the results of Doorly and Smith were obtained. A closed spot, containing disturbances which increased exponentially with time and travelled in both upstream and downstream directions, is evident in a study by the present authors (Brown and Smith [14]) of an initial-value problem arising from high Reynolds number flow over an isolated surface roughness (Savin et al. [15]). An adverse pressure gradient is also a feature of the recent work of Smith and Timoshin [16] where an inflection point lies close to the wall. In this case the spot develops on two time scales and contains exponentially-growing perturbations on the long time scale. The study also examines non-linear effects and those of non-parallelism.

The present study represents an extension of that of BS to include non-zero pressure gradients. A parallel-flow investigation is made of the linear disturbance evolution when the basic velocity profile is an idealisation of an inflection-point profile in the situation when the pressure gradient is adverse. There are now (see Fig. 1) two discontinuities in slope, and two governing parameters. When one of these, the pressure gradient parameter B, defined in Section 2, is zero, we have the BS situation (with certain limitations, see Section 3) and indeed for all $B < 0$, the favourable pressure gradient case, the disturbances are wavelike, although the resulting spots may be 'double' in planform. When $B > 0$, the adverse situation, there is a bounded linearly expanding region of exponentially growing perturbations (thus yielding much stronger growth than for the favourable or zero cases), possibly adjacent to a wavelike region. For a range of values of B, this region of exponentially-growing perturbations expands in both the upstream and downstream directions.

The plan of the paper is as follows. In Section 2 the piecewise linear profile is described, and the linearised Euler equations are solved for an initial-value problem. In Section 3 the limits in which the solution reduces to that of BS are discussed, and the role of the pressure-gradient parameter B is explained. In the favourable case when $B < 0$, as in Section 4, the BS spot is found to be modified to one of double form of which examples are given. In each piece of the double spot the disturbances are slowly decaying waves, with an additional 'spike' disturbance that remains even at large times. As in BS there are usually two waves at any horizontal station in the spot, but in the case of overlap of the double spot there may be more. The asymptotic analysis here is of stationary phase type as in BS. The situation $|B| \ll 1$ is amenable to further analysis and is the subject of Section 5. If $B < 0$ the spot splits into the double configurations of Section 4, but if $B > 0$, corresponding to an adverse pressure gradient, the decaying wavelike disturbances are separated by an almost circular region of exponentially-growing perturbations which, as B increases, eventually fill the whole spot. For $B > 0$, the asymptotic analysis involves evaluating the Fourier integral on paths through saddle points in a complex plane. This was also a feature of the papers of Brown and Smith [14] and Smith and Timoshin [16] noted above. In Section 6, the subsidiary parameter Y, defined in Section 2, is taken to be 0.5 for illustration, and spot shapes are presented for various values of B, both in the favourable and adverse pressure-gradient situations. Many of

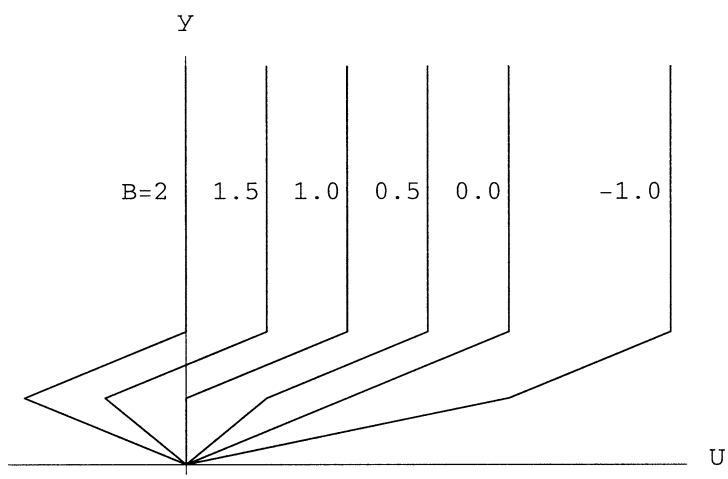

Fig. 1. The piecewise linear profile $U(y)$ for $Y = 0.5$ and various values of B. When $B = 1.5, 2$ there is a region of reversed flow.

the results are best illustrated graphically. The exponentially-growing perturbations are illustrated, in Section 7, by contour and three-dimensional plots of the pressure on the wall at a non-dimensional time $t = 20$. These are obtained from direct numerical integration of the Fourier integral. This section concludes with a part-qualitative and part-quantitative comparison of the spot-spreading angle as a function of pressure-gradient parameter with the experimental results described by Gostelow et al. [8] and D'Ovidio et al. [9,10].

Brief conclusions follow in Section 8, where further links with the experiments of Gostelow and co-workers [8–10] and with some recent ones by Narasimha [17] are noted.

2. The solution of the linearised disturbance equation, given a piecewise linear profile

The equations to be solved for a small perturbation to the prescribed streamwise profile $U(y)$ are the linearised Euler equations. If (x, y, z) are Cartesian coordinates in the streamwise, normal and spanwise directions, and $(U + u, v, w)$ are the corresponding velocity components, then the equations are

$$u_t + Uu_x + vU_y = -p_x, \qquad v_t + Uv_x = -p_y, \qquad w_t + Uw_x = -p_z, \qquad u_x + v_y + w_z = 0. \tag{1}$$

In addition, t is the time and p the pressure, in non-dimensional form.

The basic profile $U(y)$ is chosen to model boundary-layer flow along a body situated at $y = 0$, but is yet one for which Eq. (1) have an analyzable solution. Thus we take the piecewise linear profile

$$U(y) = \begin{cases} a_1 y, & 0 \leqslant y \leqslant y_1, \\ a_2 y + a_3, & y_1 \leqslant y \leqslant y_2, \\ a_4, & y_2 \leqslant y, \end{cases} \tag{2}$$

since by choice of the constants, in particular the ratio a_1/a_2, (2) can be regarded as a model for an inflection-point profile which then, as the pressure gradient becomes increasingly adverse, exhibits flow reversal. Favourable pressure gradients are also accommodated.

Since the profile in (2) is to be continuous, the constants a_1 to a_4 are related by

$$a_1 y_1 = a_2 y_1 + a_3, \qquad a_4 = a_2 y_2 + a_3 \tag{3}$$

which means that a_3, a_4 may be eliminated. It will be convenient to write

$$a_1/a_2 = 1 - B, \qquad y_1/y_2 = Y, \tag{4}$$

and assume that a_2 and y_2 are positive, whereupon B and Y remain as the two parameters of the problem. For fixed Y, with $0 \leqslant Y \leqslant 1$, and $O(1)$ values of B, the case $B < 0$ represents a *favourable* pressure gradient, and $B > 0$ an *adverse* one. At $B = 1$ the flow reverses. A representative set of profiles is illustrated in Fig. 1 for $Y = 0.5$ and various values of B. Those with $-1 \leqslant B \leqslant 1$ are fully attached, but those with $B = 1.5, 2$ exhibit a region of reversed flow near the wall.

The Fourier transform $\hat{v}(\alpha, \beta, y)$ is defined by

$$v(x, y, z, t) = \frac{1}{4\pi^2} \int_{-\infty}^{\infty} \int_{-\infty}^{\infty} \hat{v}(\alpha, \beta, y) \exp\bigl[\mathrm{i}(\alpha x + \beta z - \omega t)\bigr] \,\mathrm{d}\alpha \,\mathrm{d}\beta \tag{5}$$

with the result that the analogous $\hat{u}, \hat{w}, \hat{p}$ may be eliminated from the transforms of Eq. (1) to leave $\hat{v}$ satisfying Rayleigh's equation

$$\hat{v}_{yy} - \hat{v}\left(\alpha^2 + \beta^2 + \frac{\alpha U_{yy}}{\alpha U - \omega}\right) = 0 \tag{6}$$

with

$$\hat{v} = 0 \quad \text{at } y = 0 \text{ and as } y \to \infty. \tag{7}$$

There are also the requirements that $\hat{v}$, $\hat{p}$ must be continuous at $y = y_1, y_2$. From Eq. (1) it follows that

$$\bigl(\alpha^2 + \beta^2\bigr)\hat{p} = \mathrm{i}\alpha U_y \hat{v} - (\alpha U - \omega)\mathrm{i}\hat{v}_y \tag{8}$$

which implies that both

$$\hat{v} \quad \text{and} \quad (\omega - \alpha U)\hat{v}_y + \alpha \hat{v} U_y \tag{9}$$

must be continuous at $y = y_1, y_2$.

The solution of Rayleigh's equation satisfying (7) is

$$\hat{v} = \begin{cases} A_1 \sinh \gamma y, & 0 < y < y_1, \\ A_2 \sinh \gamma y + B_2 \cosh \gamma y, & y_1 < y < y_2, \\ A_3 \exp[-\gamma y] & y_2 < y, \end{cases} \tag{10}$$

where $\gamma^2 = \alpha^2 + \beta^2$. When the constants A_1, A_2, B_2, A_3 are chosen to satisfy the continuity conditions (9), a quadratic dispersion relation is obtained for Ω, related to the frequency ω by

$$\omega - \alpha a_4 = \Omega. \tag{11}$$

This quadratic is

$$\Omega^2 \mathrm{e}^{\gamma y_2} + \Omega\left(\bar{\alpha} a_2 \sinh \gamma y_2 + c\mathrm{e}^{\gamma y_2} + \bar{\alpha}(a_1 - a_2)\mathrm{e}^{\gamma(y_2 - y_1)} \sinh \gamma y_1\right) + c\bar{\alpha} a_2 \sinh \gamma y_2 + \bar{\alpha}^2 a_2 (a_1 - a_2) \sinh \gamma (y_2 - y_1) \sinh \gamma y_1 = 0, \tag{12}$$

where $\bar{\alpha} = \alpha/\gamma$ and $c = \alpha a_2 (y_2 - y_1)$.

After solving (12) for Ω, and writing, in addition to (4),

$$\alpha = (R/y_2)\cos\varphi, \qquad \beta = (R/y_2)\sin\varphi, \qquad x = a_2 y_2 t X/2, \qquad z = a_2 y_2 t Z/2 \tag{13}$$

we finally obtain that

$$(\alpha x + \beta z - \omega t)/t = \frac{1}{2} a_2 \left\{ RX\cos\varphi + RZ\sin\varphi - G_{1,2}(R)\cos\varphi \right\}, \tag{14}$$

where the two values, $G_1(R)$, $G_2(R)$, follow from the two solutions for Ω. They are defined as

$$G_{1,2}(R) = B\left(\mathrm{e}^{-RY} \sinh RY - 2RY\right) + R(1+Y) - \mathrm{e}^{-R} \sinh R \pm \left(F(B,R,Y)\right)^{1/2}, \tag{15}$$

where

$$F(B,R,Y) = \left(C - R(1-Y) + \mathrm{e}^{-R} \sinh R\right)^2 - 4C\mathrm{e}^{-2R+RY} \sinh RY \tag{16}$$

and

$$C = B\mathrm{e}^{-RY} \sinh RY. \tag{17}$$

It is our aim in subsequent sections to calculate the evolving pressure field $p(x, y, z, t)$, using (10) and the inversion formula (5), for chosen regions of (x, y, z) and, in particular, for large values of t and fixed X, Z in (13). For example, the pressure on the body $y = 0$ is given by

$$p(x, 0, z, t) = \sum_{j=1}^{2} \frac{1}{4\pi^2} \int_{-\infty}^{\infty} \int_{-\infty}^{\infty} F_j(\alpha, \beta) \mathrm{e}^{\mathrm{i}(\alpha x + \beta z - \omega_j t)} \, \mathrm{d}\alpha \, \mathrm{d}\beta, \tag{18}$$

where ω_1, ω_2 correspond to the two values in (12) of Ω, defined by (11). Here $F_j(\alpha, \beta) = \mathrm{i}\omega_j A_j(\omega_j)/\gamma$ (see (10)) and $F_1(\alpha, \beta) + F_2(\alpha, \beta)$ is the transform of the initial pressure field on $y = 0$, while $-\mathrm{i}\gamma^2(\omega_1^{-1} F_1(\alpha, \beta) + \omega_2^{-1} F_2(\alpha, \beta))$ is the transform of the initial value of $v_y|_{y=0}$ which is related to the slip or displacement. Later, for illustration, we shall take

$$F_1(\alpha, \beta) = F_2(\alpha, \beta) = \mathrm{e}^{-(\alpha^2 + \beta^2)}. \tag{19}$$

Subsequently it is going to be important whether $F(B, R, Y)$ in (16) vanishes in $0 < R < \infty$ with $0 \leqslant Y \leqslant 1$ and changes sign. It is clear from (16) that $F \geqslant 0$ for these ranges of R and Y if $B < 0$, the favourable pressure gradient situation. Consequently $G_{1,2}$ in (15) remain real and p in (18) will remain bounded. If $B > 0$, on the other hand, it is possible that the perturbations increase exponentially. Before embarking on this investigation, which involves a combination of asymptotic and numerical techniques, we examine the limits in which the results of this section reduce to those of earlier studies, in particular to those of Doorly and Smith [11] and of BS.

3. Limiting cases

Examination of the profiles of Fig. 1 leads one to suspect that in the limits $Y = 0, 1$ and $B = 0, \pm\infty$ the model flow considered by BS, in which there is no discontinuity in the profile slope at $y = y_1$, is attained. We explain here the sense in which this statement is correct. We take $G_1(R)$ in (15) to correspond to the positive square root of $F(B, R, Y)$ and the limits listed above respectively lead to

$$Y = 0: \quad \begin{aligned} G_1 &= 2\big(R - \mathrm{e}^{-R}\sinh R\big), \\ G_2 &= 0, \end{aligned} \tag{20}$$

$$Y = 1: \quad \begin{aligned} G_1 &= 2(1-B)R, \\ G_2 &= 2(1-B)\big(R - \mathrm{e}^{-R}\sinh R\big), \end{aligned} \tag{21}$$

$$B = 0: \quad \begin{aligned} G_1 &= \begin{cases} 2RY, & R < R_0(Y), \\ 2\big(R - \mathrm{e}^{-R}\sinh R\big), & R > R_0(Y), \end{cases} \\ G_2 &= \begin{cases} 2\big(R - \mathrm{e}^{-R}\sinh R\big), & R < R_0(Y), \\ 2RY, & R > R_0(Y), \end{cases} \end{aligned} \tag{22}$$

$$B = -\infty: \quad \begin{aligned} G_1 &= -2BRY, \\ G_2 &= -2B\big(RY - \mathrm{e}^{-RY}\sinh RY\big). \end{aligned} \tag{23}$$

In (22), $R_0(Y)$ is defined to be the solution of $2R(1-Y) = (1 - \mathrm{e}^{-2R})$, and is the zero of $F(0, R, Y)$. If, for example, $Y = 0.5$, then $R_0 = 0.796812$. If $Y \ll 1$, then $R_0 \approx Y$, but if $Y \approx 1$, then $R_0 \approx \frac{1}{2}(1-Y)^{-1}$. In (21), G_1 and G_2 should be interchanged if $B > 1$, and in (23) if $B = +\infty$.

The dispersion relation of BS corresponds exactly to G_1 in (20) and led to a single spot. A spot of strictly similar shape and size may be obtained from G_2 in (21) (by scaling X, Z with $1 - B$) and from G_2 in (23) (by scaling R with Y^{-1} and X, Z with $-BY$). Exactly the same dimension of spot may also be obtained from (22) with G_2 for $R < R_0(Y)$ and G_1 for $R > R_0(Y)$. In each case, the other G is proportional to R, say $G = X_0 R$ for constant X_0, and gives a contribution

$$\frac{1}{4\pi}\exp\left[-\frac{1}{16}a_2^2 y_2^2\big((X - X_0)^2 + Z^2\big)t^2\right] \tag{24}$$

to (18) in the case $F_1(\alpha, \beta) = F_2(\alpha, \beta) = \mathrm{e}^{-(\alpha^2+\beta^2)}$. The expression (24) represents the movement of the initial Gaussian disturbance upstream/downstream with constant speed $a_2 y_2 |X_0|/2$. It decays very rapidly with time except at the point $X = X_0$, $Z = 0$ where it remains as a 'spike' of height $(4\pi)^{-1}$ in the disturbance. This spike will be evident in some of the numerical results of Section 4. In addition to the presence of the spike in the limiting solutions, if two limits, say $B = 0$ and $B = -\infty$, are examined at the same value of the time t, although the spot is the same shape, the perturbations will be different because the factor $-B$ in (23) implies also a scaling in t.

It is reasonable to regard the BS solution as describing a zero pressure-gradient case, and for fixed Y with $0 < Y < 1$, this particular spot shape is attained at $B = -\infty, 0, \infty$. Thus it is not possible to regard B as a parameter that increases monotonically from $-\infty$ to ∞ as the pressure gradient increases. However, since the form of the profiles in Fig. 1 suggests a change of sign of pressure gradient as B increases through zero, we shall regard, for convenience, $B = 0$ as corresponding to a zero pressure gradient which, as B increases, becomes increasingly adverse, with reversed flow at $B = 1$, until $B = Y^{-1}$ when the whole flow is reversed. We also interpret a decrease of B from zero as an increasingly favourable pressure gradient, although B has some lower bound for this situation. This point is raised again in Section 7 when qualitative comparison is made with available experimental data.

4. Double spot shapes for $B < 0$ (favourable cases)

In this section we show that, when $B < 0$, spots of the BS type, but double, are obtained in the large-time limit. To achieve this we seek the asymptotic form of the inverse transforms (5) by a double steepest descent technique. From (18), to evaluate the pressure on the wall for example, we need the sum of two integrals of the form

$$\frac{1}{4\pi^2}\int_{-\infty}^{\infty}\int_{-\infty}^{\infty} \mathrm{e}^{-(\alpha^2+\beta^2)}\mathrm{e}^{\mathrm{i}(\alpha x + \beta z - \omega t)}\,\mathrm{d}\alpha\,\mathrm{d}\beta, \tag{25}$$

one for each value of ω in (11), (12) with $e^{-(\alpha^2+\beta^2)}$ representing the effect of an initial condition. The important quantity in (25) is the second exponential, and we set $X = S\cos\theta$, $Z = S\sin\theta$ in (14) and define

$$E(R, S, \theta, \varphi) = RS\cos(\theta - \varphi) - G(R)\cos\varphi \tag{26}$$

for each $G_{1,2}$. To obtain the actual exponent of interest in (25) we must multiply E by $ia_2t/2$. Since, as noted in Section 2, $F(B, R, Y)$ in (15) is non-negative for $B \leqslant 0$, E in (26) is purely real if R, φ are real and so the perturbations are bounded.

To determine the asymptotic form of the integral (25) for large t and fixed X, Z we search for saddle points successively, first in φ by using $\partial E/\partial\varphi = 0$, namely

$$RS\sin(\theta - \varphi) + G(R)\sin\varphi = 0 \tag{27}$$

so that

$$\tan\varphi = \frac{RS\sin\theta}{(RS\cos\theta - G(R))}. \tag{28}$$

On substitution of (28) into (26), E becomes

$$\overline{E}(R, S, \theta) = \pm\left(R^2S^2 - 2RSG\cos\theta + G^2\right)^{1/2} \tag{29}$$

according as $(RS\cos\theta - G(R))\cos\varphi \gtrless 0$. The positions of the saddle points are then obtained by solving $d\overline{E}/dR = 0$ with the result that the values of R are given by the equation

$$S^2 - S\cos\theta(G' + G/R) + GG'/R = 0. \tag{30}$$

In the BS case there were two real values of R inside the spot, each of which led to a wave-like contribution to (25). We now have two functions, $G_{1,2}(R)$, so may anticipate two spots. The edge/s of the spot/s will be reached where (30) has a double root, i.e., where

$$-S\cos\theta\left(G'' + (G/R)'\right) + (GG'/R)' = 0 \tag{31}$$

together with (30).

The length of the spot as measured along the X-axis may be examined as follows. With θ set equal to zero in (30) it factorises to give

$$S = G(R)/R \quad \text{or} \quad S = G'(R) \tag{32}$$

so the maximum and minimum values of S will be given by the maxima and minima of $G(R)/R$ and $G'(R)$. First, it may be shown from (15) to (17) that

$$\frac{G_1(R)}{R} \approx 2(1 - B)Y \quad \text{as } R \to 0,$$

and

$$\frac{G_1(R)}{R} \approx 2(1 - BY) \quad \text{as } R \to \infty, \tag{33}$$

the same asymptotes holding for $G_1'(R)$. Also

$$\frac{G_2(R)}{R} \approx \frac{2(1 - BY)^2}{1 - B}R \quad \text{as } R \to 0,$$

and

$$\frac{G_2(R)}{R} \approx 2(1 - B)Y \quad \text{as } R \to \infty. \tag{34}$$

Thus if $G_{1,2}/R$ and $G_{1,2}'$ are monotonic we expect that the G_2 spot terminates at $X = 0$ and extends to $X = 2(1 - B)Y$, and that the G_1 spot lies in front of it, i.e., at larger values of X, terminating at $X = 2(1 - B)Y$ and extending to $X = 2(1 - BY)$. The latter position, $X = 2(1 - BY)$, corresponds to the speed a_4 at the outer edge of the profile, the position $X = 2(1 - B)Y$ to the speed at the slope discontinuity at $y = y_1$, and $X = 0$ to that at the wall which is at rest (see Fig. 1). The trailing-edge angle of each part of the composite spot is the same, namely $\tan^{-1}(8^{-1/2})$ as for the BS spot. This may be shown by letting $R \to 0$ in (30), (31) and using (33), (34). It is found on eliminating R, that as $R \to 0$, for the leading spot the shape of its trailing edge is given by

$$\left(X - 2(1 - B)Y\right)^2 = 8Z^2 \tag{35}$$

while for the rear spot with its trailing edge at the origin the BS result $X^2 = 8Z^2$ holds.

The behaviour of $G_{1,2}/R$ and $G'_{1,2}$ depends on the values of B and Y. Although G_1/R and G'_1 are monotonic for the values that have been considered, G_2 leads to anomalous behaviour. Indeed for $Y > 0.5$, it may be shown that, as $R \to \infty$, $G'_2 \to 2(1-B)Y$ from above, so that the rear spot will overshoot $X = 2(1-B)Y$ (the trailing edge of the leading spot), and that if $Y < 0.5$, G'_2 may tend to its limit from below but not be monotonic so that there are extra roots (or subspots) inside the trailing spot. The situations are illustrated in Fig. 2 in which, from the top, are considered the values $(-0.5, 0.25)$, $(-0.2, 0.25)$ and $(-0.2, 0.75)$ of the parameters (B, Y). In Fig. 2(a) is plotted $G_{1,2}/R$ and $G'_{1,2}$ for the three cases, and in Fig. 2(b) the double spot shapes obtained by solving (30), (31) successively with $G = G_{1,2}$ are shown. Since $B < 0$, the pressure gradient of the basic profile is favourable and the flow entirely forward (see Fig. 1). Also, from (13), the coordinates X, Z represent

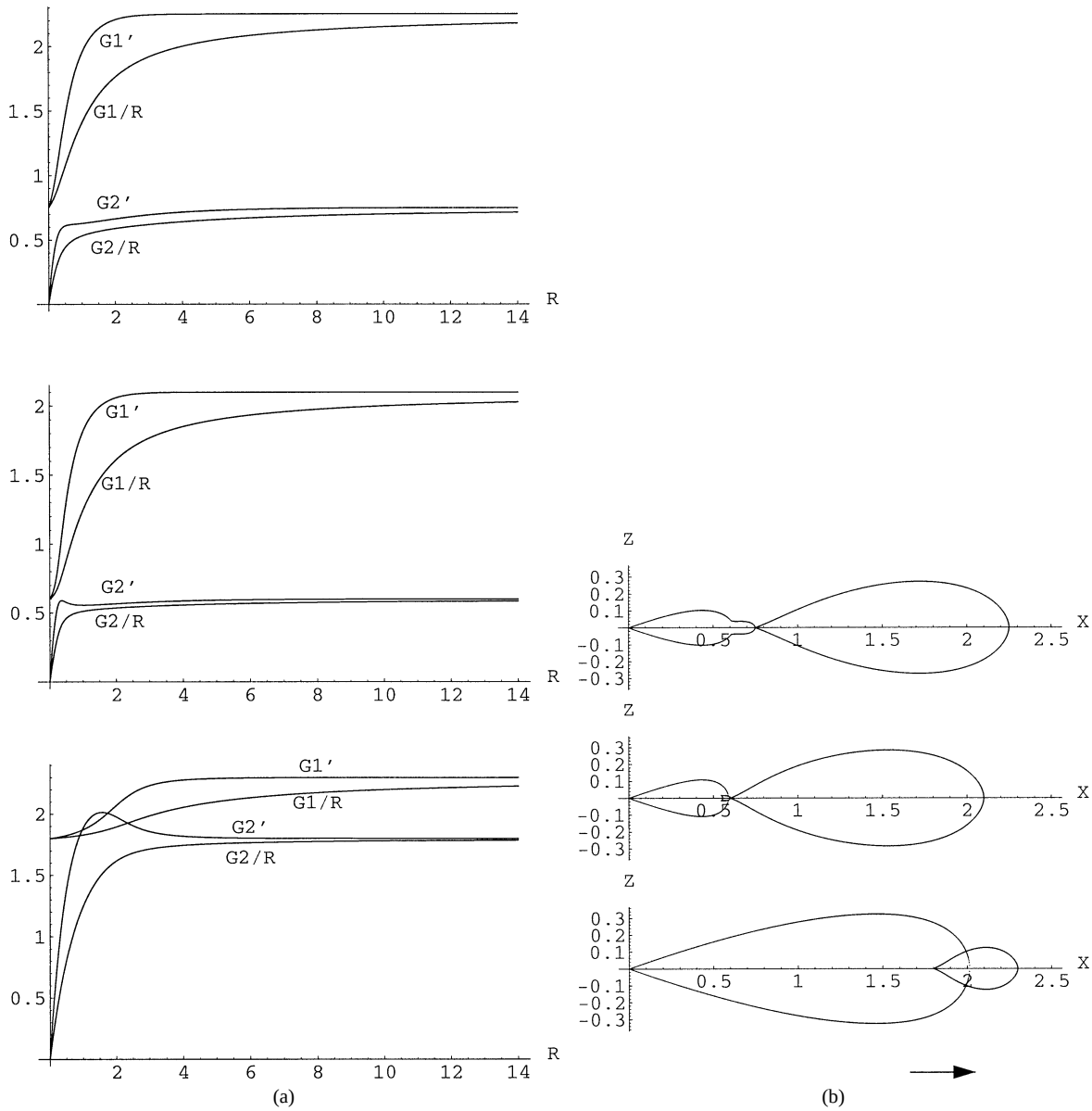

Fig. 2. (From top) $B = -0.5,\ Y = 0.25$, then $B = -0.2,\ Y = 0.25$, then $B = -0.2,\ Y = 0.75$. (a) $G'_{1,2},\ G_{1,2}/R$. (b) Double spot shapes. The spots are expanding spanwise and in the $X > 0$ (downstream) direction. The spot boundaries are obtained by simultaneously solving (30) and (31) with (15), and separate the regions of oscillatory wall-pressure perturbations from the main body of the fluid where they decay exponentially.

velocities; thus the double spots illustrated in Fig. 2(b) have a fixed trailing edge at the origin and a leading edge that has a forward motion in the positive x-direction at the speed of the outer part of the profile. The perturbation spreads spanwise as the spot expands in the downstream direction. When $B=-0.5$, $Y=0.25$ all four functions in Fig. 2(a) are monotonic, and the spot shape in Fig. 2(b) shows no overlapping or subspots. As predicted, the leading spot extends from $X=2.25$ to $X=0.75$, and the trailing spot from $X=0.75$ to $X=0$. When $B=-0.2$, $Y=0.25$, as shown in Fig. 2(a), G_2' has a maximum and a minimum with values below its limit at $R=\infty$ and this leads to the very small subspot visible in Fig. 2(b) at values of X just less than 0.6. However, when $B=-0.2$, $Y=0.75$, the maximum of G_2' is greater than the $R=\infty$ limit and the trailing spot overlaps the leading one. The closure of spots or subspots is caused by the vanishing of one or other of the G'' values. The leading edge of the configuration is provided by G_1 in the limit $R\to\infty$, and is of parabolic form with a logarithmic modification similar to that in BS namely

$$Z^2 \propto (X_L - X)/\ln\left(\frac{1}{X_L - X}\right), \tag{36}$$

where $X_L = 2(1-BY)$. If there is no overlap or subspot (as for $B=-0.5$, $Y=0.25$ in Fig. 2) the trailing spot also has leading edge of the form (36), with $X_L = 2(1-B)Y$. Closures which are caused by the vanishing of G_2'' at finite R, say $R=\rho_0$ (as in the other examples in Fig. 2), are purely parabolic in the limit with

$$Z^2 \approx \big(G_0' - X\big)\big(G_0' - G_0/\rho_0\big), \tag{37}$$

where $G_0 = G_2(\rho_0)$, $G_0' = G_2'(\rho_0)$.

We conclude this section by plotting in Fig. 3 the lines of constant wall pressure corresponding to the spot shapes illustrated in Fig. 2. Also shown are three-dimensional plots of the perturbation. The computations were carried out using the results of the double saddle-point argument of this section. For given X, Z the real positive values of R that satisfy (30) are calculated (in general just two for each function $G(R)$), and the integrals (25) are written in the polar coordinates defined by (13). The values of φ corresponding to the real values of R are obtained from (28). It is then necessary to evaluate the sum

$$\frac{1}{\pi t}\sum \frac{\mathrm{Re}^{-R^2}}{|ca-b^2|^{1/2}}\cos\left(\frac{t}{2}E + \frac{\pi}{4}\operatorname{sgn} a(1+\operatorname{sgn} \mathrm{d})\right) \tag{38}$$

taken over both functions $G(R)$ and corresponding pairs (R,φ) obtained from (30) and (28) with $|\varphi|<\pi/2$. Here E is defined by (26) and a, b, c, d by

$$a = -\frac{1}{2}G''(R)\cos\varphi, \qquad b = \frac{1}{2}\big(S\sin(\theta-\varphi) + G'(R)\sin\varphi\big), \qquad c = -\frac{1}{2}E, \qquad d = ca - b^2 \tag{39}$$

and we have taken $a_2 = y_2 = 1$. The expression (38) is equivalent to (4.1) of BS.

Fig. 3 is concerned with $t=20$ and the same values of B and Y as in Fig. 2, namely $(B,Y) = (-0.5, 0.25), (-0.2, 0.25), (-0.2, 0.75)$ in order from the top. In Fig. 3(a) the double spot appears to have a gap when $B=-0.5$, $Y=0.25$ but this is only because the perturbation right at the leading edge of the trailing spot is very small. However in the corresponding illustration in Fig. 3(b), which is a view from the rear, the magnitude of the perturbation in the neighbourhood of the protuberance is roughly seven times the maximum perturbation elsewhere. When $B=-0.2$, $Y=0.25$ there is a subspot generated by G_2. The magnitude of the perturbation in this subspot, shown from the front in Fig. 3(b), is about ten times that at the spot perimeter. In addition, when $B=-0.2$, $Y=0.75$, the maximum perturbation occurs in the overlap region and otherwise there is very little in the small leading spot. The lowest diagram in Fig. 3(b) is a view from the front for this last case, and shows that the maximum perturbation is almost fifteen times that elsewhere.

The value of $B=-0.2$ with $Y=0.25, 0.75$ in Fig. 3 was chosen to illustrate the occurrence of a subspot and an overlap. However, the relatively small value of $-B$, namely 0.2, means that the solution is fairly near the BS limit $B=0$. In this limit, as noted in Section 3, the pressure contours are the same as theirs for all $0 \leqslant Y \leqslant 1$ but with the addition of a 'spike' of height $(4\pi)^{-1}$ at the point $X=2Y$, $Z=0$ which corresponds to the speed of the point of slope discontinuity at $y=y_1$. In Fig. 3(b) this spike is clearly seen, although its height is overestimated by the asymptotic form (38) which predicts strictly unbounded perturbations at the caustic. In the illustrations at the top of Fig. 3, where neither B nor Y is particularly close to a BS limit, the largest perturbations are somewhat distributed over the trailing smaller spot. For illustration, we also include Fig. 4 for $B=-10^{-6}$, $Y=0.5$ and $t=20$ which is very close to the limit. In Fig. 4(a) the contours shown are essentially identical to those of BS, the circle containing the additional roots which are to be discussed in the following section, and the location of the spike, at $X=2Y=1$ (Fig. 4(b)) being clearly visible. If Fig. 4(a) is repeated with $B=10^{-6}$ the results are indistinguishable graphically: in particular, the circles are identical, although, as shown below, when $B>0$ the perturbation within it actually increases exponentially with time.

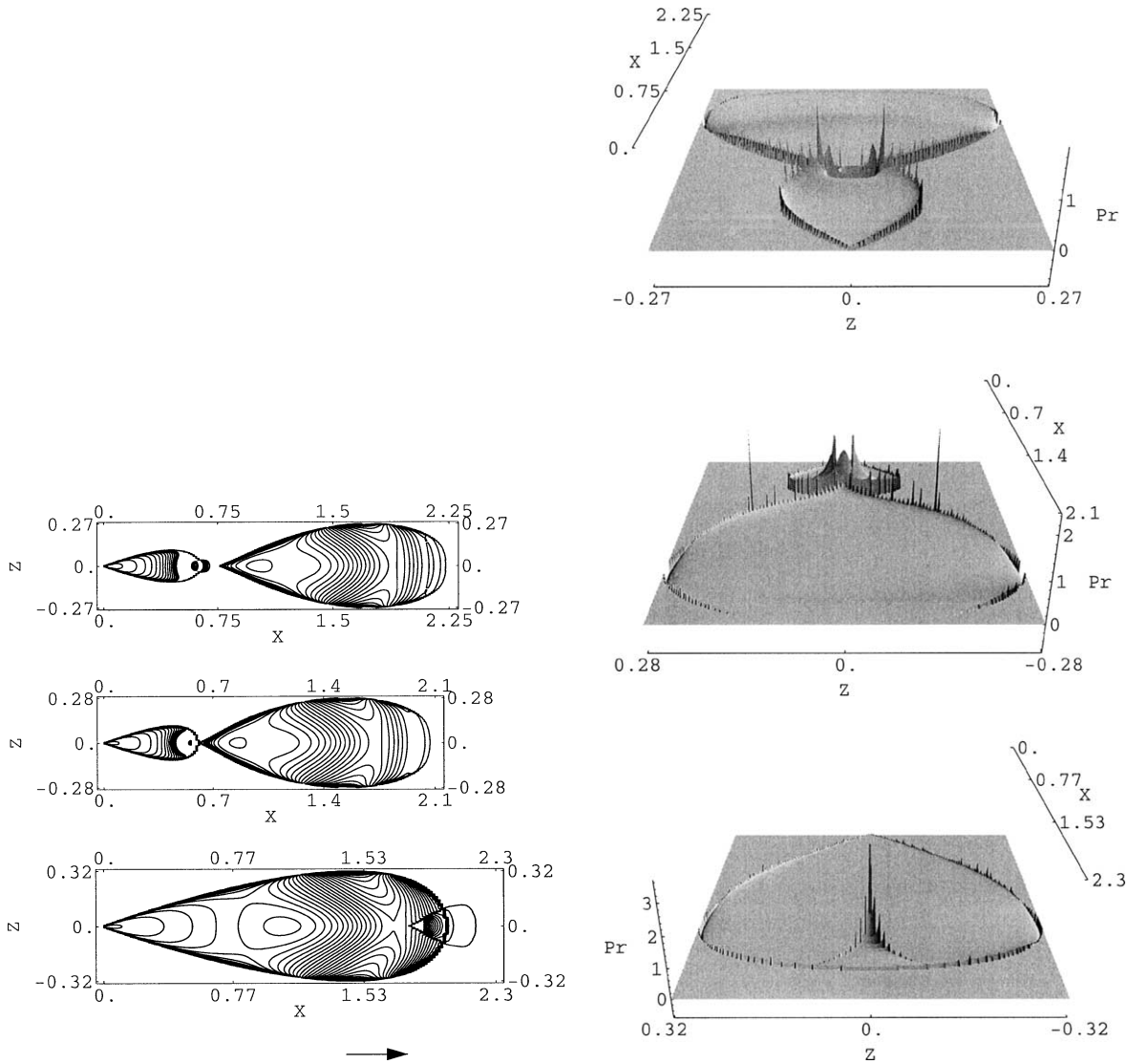

Fig. 3. (From top) $B=-0.5$, $Y=0.25$, then $B=-0.2$, $Y=0.25$, then $B=-0.2$, $Y=0.75$ as in Fig. 2 and $t=20$. (a) Contour lines for the wall pressure. (b) The wall-pressure distribution (times π). The top is a view from the rear of the configuration and the others are views from the front (i.e., respectively, from $X<0$ and $X>0$ in (a)).

5. The adverse/favourable pressure gradient divide

The adverse and favourable pressure gradient situations corresponding to the profiles in Fig. 1 are divided by the value $B=0$. In this limit, it is clear from (22) that $G'_{1,2}$ are discontinuous at $R=R_0(Y)$ where $R_0(Y)$ satisfies

$$2R_0(1-Y)=1-\mathrm{e}^{-2R_0} \tag{40}$$

and is the zero of $F(0,R,Y)$ in (16). Indeed, G'_1 jumps up from $2Y$ to $2(1-\mathrm{e}^{-2R_0(Y)})$ and G'_2 makes the same jump downwards. We write this jump as 2Δ so that

$$\Delta=1-Y-\mathrm{e}^{-2R_0}, \tag{41}$$

which may be shown to be positive on use of (40), and for convenience define

$$\Gamma=1+Y-\mathrm{e}^{-2R_0}. \tag{42}$$

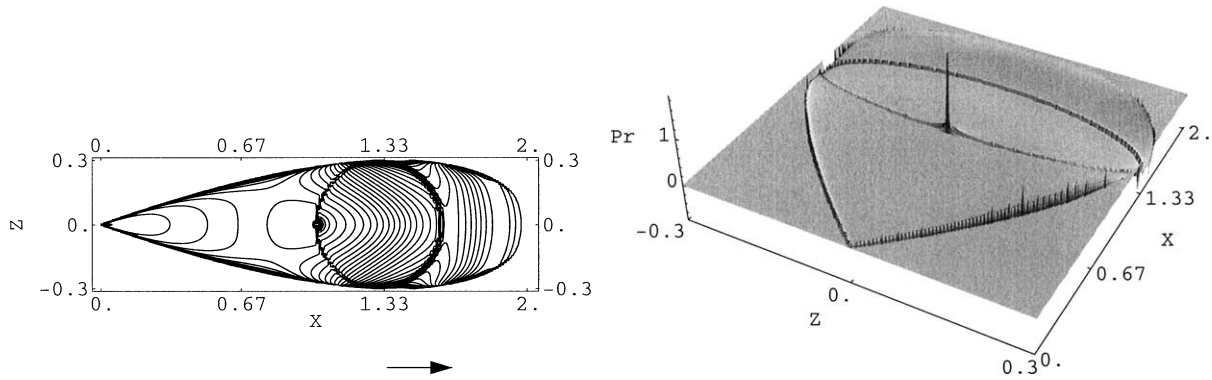

(a) (b)

Fig. 4. $B = -10^{-6}$, $Y = 0.5$ and $t = 20$. (a) Contour lines for the wall pressure. (b) A view from the rear of the spot. The wall pressure perturbation is Pr/π. This illustrates the BS limit as $B \to 0^-$ together with the residual "spike."

If Eqs. (30) and (31) for the spot boundary are solved with $G_2 = 2(R - \mathrm{e}^{-R}\sinh R)$ for $R < R_0(Y)$ and the curve is drawn in the XZ-plane, this curve is the trailing-edge portion of the BS spot. Similarly the leading-edge portion is obtained by using $G_1 = 2(R - \mathrm{e}^{-R}\sinh R)$ for $R > R_0(Y)$. The easiest way to find these curves numerically is to regard R as a parameter along the curve and use (31) to determine $X\ (= S\cos\theta)$ and then (30) to determine $Z(= S\sin\theta)$. The two portions together form the BS spot and the curve at the junction $R_0(Y)$ is continuous and differentiable.

We now show that as $|B|$ increases from zero, the circle visible in Fig. 4(a) forms inside this BS spot, with radius and centre depending on Y, in which extra roots of Eq. (30) for the saddle points appear. For the $B = 0$ limit of BS, there are two roots at each interior point, either two with $R < R_0(Y)$ or two with $R > R_0(Y)$ or one of each. However, as soon as $|B|$ becomes greater than zero two extra roots appear inside the circle. If $B < 0$ the new roots are real and the BS single spot starts to form a double spot initially of the overlapping type discussed in Section 4. However, if $B > 0$, the adverse situation, the result is quite dramatic as the extra roots are now complex, and the original spot now splits into two pieces in which the perturbations remain oscillatory but separated by a small region in which the disturbance grows exponentially with time. As B increases, the size of the region, initially circular, also increases.

Before illustrating the situation numerically with a chosen value $Y = 0.5$, we show how this circle containing the additional roots arises. The arguments for $B \gtrless 0$ are similar so we first take $B \to 0^-$, then note the differences for $B \to 0^+$.

5.1. The additional roots as B decreases from zero

In the limit $B \to 0$, $F(B, R, Y)$ in (16) vanishes at $R = R_0(Y)$ and to smooth out the discontinuity in $G'_{1,2}$ described by (40), (41) we write

$$R - R_0(Y) = (-B)^{1/2}T \tag{43}$$

as $B \to 0^-$. Thus

$$F(B, R, Y) \approx (-B)\Delta^2\left(T^2 + \lambda^2\right), \tag{44}$$

where Δ is defined in (41) and

$$\lambda^2 = \mathrm{e}^{-2(1-Y)R_0}\left(1 - \mathrm{e}^{-2YR_0}\right)^2/\Delta^2. \tag{45}$$

If the term $O(R - R_0)$ in (15) is retained it follows that

$$G_{1,2} \approx 2R_0Y + \Gamma(-B)^{1/2}T \pm (-B)^{1/2}\Delta\left(T^2 + \lambda^2\right)^{1/2} \tag{46}$$

with the final term being the contribution from $F^{1/2}$ for $G_{1,2}$, respectively. From (46) we therefore have

$$G'_{1,2} \approx \Gamma \pm \frac{\Delta T}{(T^2 + \lambda^2)^{1/2}} \tag{47}$$

so that, as required

$$G'_{1,2} \approx \Gamma \mp \Delta \quad \text{as } T \to -\infty \quad \text{and} \quad G'_{1,2} \approx \Gamma \pm \Delta \quad \text{as } T \to +\infty. \tag{48}$$

If (45) and (46) are now substituted into (30), the equation for the position of the saddle point/s giving T as a function of S and θ, it becomes

$$S^2 - S\cos\theta\left(2Y + \Gamma \pm \frac{\Delta T}{(T^2+\lambda^2)^{1/2}}\right) + 2Y\left(\Gamma \pm \frac{\Delta T}{(T^2+\lambda^2)^{1/2}}\right) = 0. \tag{49}$$

From (49), on rearranging, we obtain

$$\pm\frac{\Delta T}{(T^2+\lambda^2)^{1/2}} = \widetilde{B}/\tilde{A}, \tag{50}$$

where $\tilde{A}$ and $\widetilde{B}$ are defined by

$$\tilde{A} = S\cos\theta - 2Y = X - 2Y, \qquad \widetilde{B} = S^2 - S\cos\theta(2Y+\Gamma) + 2Y\Gamma = \left(X - \left(\Gamma - \frac{\Delta}{2}\right)\right)^2 + Z^2 - \frac{\Delta^2}{4}. \tag{51}$$

From (50) it follows that

$$T^2 = \frac{\lambda^2\widetilde{B}^2}{\Delta^2\tilde{A}^2 - \widetilde{B}^2} \tag{52}$$

which yields real saddle points in the neighbourhood of $R = R_0$ if the denominator in (52) is positive. This condition is

$$\left(\left(X - (\Gamma - \Delta)\right)^2 + Z^2\right)\left(\Delta^2 - (X-\Gamma)^2 - Z^2\right) > 0 \tag{53}$$

and is satisfied inside the circle

$$(X-\Gamma)^2 + Z^2 = \Delta^2, \tag{54}$$

where also $\tilde{A} > 0$ since the diameter of the circle on the X axis is from $\Gamma - \Delta(= 2Y)$ to $\Gamma + \Delta$.

The solutions of (50) may now be written as

$$T = \pm\frac{\lambda\widetilde{B}}{(\Delta^2\tilde{A}^2 - \widetilde{B}^2)^{1/2}}, \tag{55}$$

where the positive sign yields the saddle point corresponding to G_1, and the negative sign yields that corresponding to G_2.

5.2. The additional roots as B increases from zero

The argument leading to additional roots in the same circle as given by (54) follows as for $B < 0$, but now the extra roots are complex. The definition for T in (43) is replaced by

$$R - R_0(Y) = B^{1/2}T \tag{56}$$

so that

$$F(B,R,Y) \approx B\Delta^2\left(T^2 - \lambda^2\right) \tag{57}$$

with λ again given by (45). Eq. (46) is replaced by

$$G_{1,2} \approx 2R_0Y + \Gamma B^{1/2}T \pm B^{1/2}\Delta\left(T^2-\lambda^2\right)^{1/2}, \tag{58}$$

and (47) by

$$G'_{1,2} \approx \Gamma \pm \frac{\Delta T}{(T^2-\lambda^2)^{1/2}}. \tag{59}$$

In Eq. (49), λ^2 must be replaced by $-\lambda^2$ and (50), (52) are now

$$\pm\frac{\Delta T}{(T^2-\lambda^2)^{1/2}} = \widetilde{B}/\tilde{A}, \qquad T^2 = \frac{-\lambda^2\widetilde{B}^2}{\Delta^2\tilde{A}^2 - \widetilde{B}^2}. \tag{60}$$

The roots we seek now are complex, for if they exist there is a possibility of an exponential contribution to the integrals of the form (18) at large values of the time. Thus again we require X, Z to lie inside the circle defined by (54) and

$$T = \pm\frac{\mathrm{i}\lambda\widetilde{B}}{(\Delta^2\tilde{A}^2 - \widetilde{B}^2)^{1/2}}. \tag{61}$$

The cut/s in the T-plane for the function $(T^2-\lambda^2)^{1/2}$ may be taken as we please. Since G_1, G_2 occur symmetrically in the solution (18) with (19), i.e., they may be interchanged in any range of R without altering (18), the final answer is unaltered. To achieve the discontinuities in (48) as $|T| \to \infty$ we may cut from λ to $\lambda - \mathrm{i}\infty$ and from $-\lambda$ to $-\lambda + \mathrm{i}\infty$ and take $(T^2-\lambda^2)^{1/2} \approx |T|$ as $|T| \to \infty$ along the real axis; then on the imaginary axis $(T^2-\lambda^2)^{1/2}$ is pure imaginary.

5.3. *Illustration of the additional roots in the case* $Y = 0.5$

The theory of the preceding subsections is illustrated here in the particular case of $Y = 0.5$. When $B = 0^-$, the additional roots in the circle defined by (54) are real and positive and are thus on the path of integration of (25) in the polar co-ordinates R, φ. Thus all that is required is numerical confirmation of their existence, and a demonstration of their effect on the development of the spot. However, when $B = 0^+$, these roots are in the complex R-plane and it is necessary to consider the validity of deforming the path of integration through these saddle points. Since it is exponentially large contributions to (25) that are of interest, we examine those saddle points (61) which lead to a positive real part in $\mathrm{i}\overline{E}$ in (29), and plot the lines in the complex T-plane on which $\mathrm{re}(\mathrm{i}\overline{E})$ is constant to ensure that there is an acceptable path from $T = -\lambda$ to $T = \lambda$ through the saddle point. This path must lie in the valleys, and on it $\mathrm{re}(\mathrm{i}\overline{E})$ must take values less than that at the saddle point. For the contribution from $G_1(R)$, for example, the curve through the saddle point that divides hills from valleys is

$$\begin{aligned}&\mathrm{re}\{\mathrm{i}(TS^2 - S\cos\theta(T(2\Gamma - \Delta) + \Delta(T^2 - \lambda^2)^{1/2}) + 2Y(T\Gamma + \Delta(T^2 - \lambda^2)^{1/2}))\}\\ &\quad = \lambda(\Delta^2\tilde{A}^2 - \widetilde{B}^2)^{1/2}\end{aligned} \tag{62}$$

for values of X, Z inside the circle (54). Confirmation of an acceptable path has been made when $Y = 0.5$ for a selection of values of X, Z although the results are not presented here. Additional confirmation is provided by direct evaluation of the Fourier integrals (25) described in Section 7.

In Fig. 5 we illustrate the breaking of the BS spot as $|B|$ increases from zero for the value $Y = 0.5$. For $Y = 0.5$, $R_0 = 0.796812$, $\Delta = R_0 - 0.5$, $\Gamma = R_0 + 0.5$ and the circle (54) has centre at $X = 1.296812$ and radius 0.296812. The circle can be seen clearly in both diagrams which are obtained by seeking the equal root curves defined by (30), (31). The circle is where the extra roots (over those of the $B \equiv 0$ case) become equal. In Fig. 5(a), where $B = -0.0001$, there are two real roots, and thus two waves given by G_1 in the region outside the circle and nearer the leading edge, two given by G_2 in the trailing region and four waves inside the circle (two from each of G_1 and G_2). In Fig. 5(b), where $B = 0.0001$, $F(B, R, Y) < 0$ for $0.785 < R < 0.809$ and the two pieces of the BS spot have separated. In the piece nearer the leading edge there are still two waves given by G_1, and in that nearer the trailing edge there are two given by G_2. In the roughly circular piece between, the perturbation increases exponentially with time, as a result of the complex saddle points through which the path of integration is deformable. The region is bounded above and below, as well as laterally by the circle, and in the following section the missing piece of boundary is determined.

6. Spot shapes for $Y = 0.5$ and various values of the pressure gradient parameter B

The spot shape when $B = 0$ is that of BS and differs very little from that in Fig. 5(a). As B decreases and the pressure gradient becomes favourable, the double-spot shape becomes evident and the overlap gradually disappears. For illustration, two further negative values of B are shown in Fig. 6. For $0 > B > -0.175$, the leading hump of the spot is fractionally wider, at $B = -0.175$, as in Fig. 6(a), the two humps are of the same width, but when B reaches -5.0, as in Fig. 6(b) the rear hump is dominant and is well on its way to the BS limit again as $B \to -\infty$. The crescent-shaped spot on the axis at $X = 2(1 - B)Y$ in Fig. 6(a) is a consequence of the overshoot of the trailing spot from its position predicted by $R = \infty$. This point is also the site, in the limit $B \to 0^-$, of the 'spike' perturbation noted in Section 3.

As B increases from zero and the pressure gradient becomes adverse, the spot splits into two distinct pieces containing *oscillatory* contributions to the disturbance, but separated by an initially circular region in which the perturbation increases

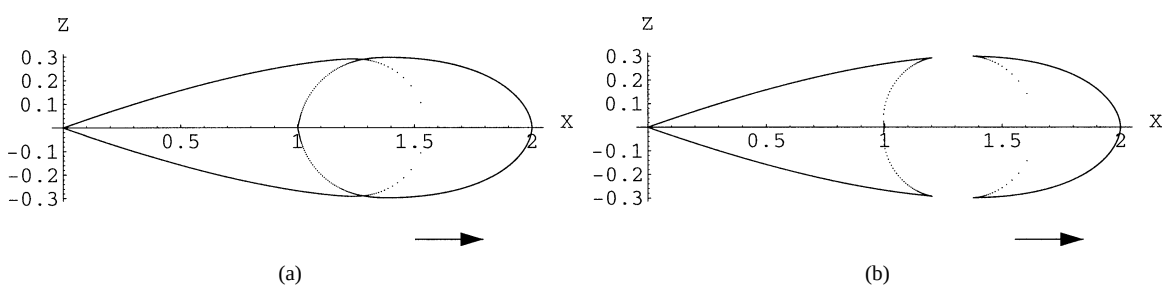

Fig. 5. The favourable/adverse pressure gradient divide with $Y = 0.5$. (a) $B = -0.0001$, and the near circle containing the additional real roots. The spot is becoming double with an overlap region. (b) $B = 0.0001$ and the near circle containing the complex roots. The regions containing waves are separated by one containing exponentially large wall-pressure perturbations. The closed curves are obtained as in Fig. 2(b).

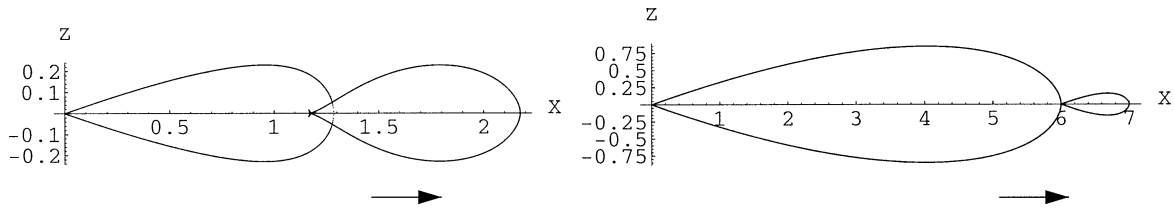

(a) (b)

Fig. 6. The double spots when $Y = 0.5$. (a) $B = -0.175$, and the two pieces are of the same width. (b) $B = -5.0$, and the BS limit at $B = -\infty$ is being approached. The closed curves are obtained as in Fig. 2(b) and wall-pressure perturbations are oscillatory in the interiors.

exponentially with time. The split is illustrated for $B = 0.0001$ in Fig. 5(b). There is a boundary that separates this region from the general body of the fluid in which the perturbation is decaying exponentially. This boundary is determined by finding the curve for which Eq. (30) (the saddle-point condition) holds, together with the requirement that $\overline{E}$ in (29) is real. The latter is equivalent to requiring that

$$\mathrm{im}\left(R^2S^2 - 2RSG\cos\theta + G^2\right) = 0 \tag{63a}$$

and

$$\mathrm{re}\left(R^2S^2 - 2RSG\cos\theta + G^2\right) > 0. \tag{63b}$$

To obtain the curve, the value of X was specified, and that of Z estimated. Eq. (30) was then solved for the appropriate (complex) values of R, and then Z was determined by fixed point iteration on (63a) with $S^2 = X^2 + Z^2$. Eq. (63b) was used as a check. With a reasonably accurate first guess for Z and R the procedure worked well and results are shown in Fig. 7. In Fig. 7(a), $B = 0.1$ and there is little left of the leading oscillatory region (see mention of Gostelow's bow-wave in Sections 7 and 8), and in Fig. 7(b), where $B = 1.0$, the spot is completely unstable and is almost circular. It is at this value of B that the basic flow is about to reverse. In Fig. 7(c), with $B = 1.5$, flow reversal has occurred, the disturbance travels both upstream and downstream and the flow has become absolutely unstable. The final diagram, Fig. 7(d), has $B = 1/Y = 2.0$ at which value of B the mainstream is about to reverse. Now the disturbance is spreading in the upstream direction only. Higher values of B in this model eventually lead to $B = \infty$ and the BS limit again. Hence Fig. 7(d) is regarded as the final illustration of interest in the present context.

In the following section we present pressure profiles for the values of B for which the spot shapes are shown in Fig. 7. Also, similarities are noted between the laminar spots described here, and turbulent spots observed experimentally in a boundary layer undergoing transition.

7. The exponentially growing perturbations

The perturbations to the pressure and velocity components grow exponentially inside part of the spot boundary for $0 < B < 1$, and inside all of it for $1 \leqslant B \leqslant 2$. In Fig. 8 we illustrate this by contour and three-dimensional plots for $Y = 0.5$, $t = 20$ and $B = 0.1, 1.0, 1.5$ and 2.0, respectively, for which the spot outlines are shown in Fig. 7. The quantity shown is $4\pi^2$ times the pressure on the wall and is calculated by direct numerical evaluation of the inverse Fourier transforms in (25) written in terms of the coordinates defined by (13) and with the exponent given by (14). This approach is in contrast to that employed to produce Fig. 3 for values of $B < 0$ where the asymptotic expansion (38) was employed. For values of $B > 0$, the asymptotic analysis is invaluable for predicting the splitting of the spot as $|B|$ increases from zero, and for establishing the outline. However, to use it for general values of X, Z it is necessary to solve (30) for the complex saddle point R and then to evaluate $\overline{E}$ in (29) at this value of R. Since $G_{1,2}$ involve both exponential functions and a square root, there are many branch points in the complex R-plane, and many solutions to (30). Also the correct root for $\overline{E}$ in (29) must be selected and finally it should be verified that the path of integration may be deformed from the real R-axis to pass through the saddle point. For small values of B this was carried out, as described in Section 5, but for larger $B > 0$ it was felt that the chance of switching to an unwanted root of (30), or to a wrong square root, was too great. Thus, apart from a comparison between the two approaches for representative values of X, Z and B, carried out for checking purposes, the integrals in (25) were evaluated directly.

Although the contour and three-dimensional plots of Fig. 8 are obtained by evaluation of the full integrals at $t = 20$, it is clear the spot shapes and properties of Fig. 7 as predicted by the large-time asymptotic analysis are being attained. Each exponentially growing perturbation to the wall pressure is very different from the decaying oscillations for the negative values of B shown in Fig. 3. They are however, except in magnitude, very similar to each other. In each case the maximum perturbation occurs on the

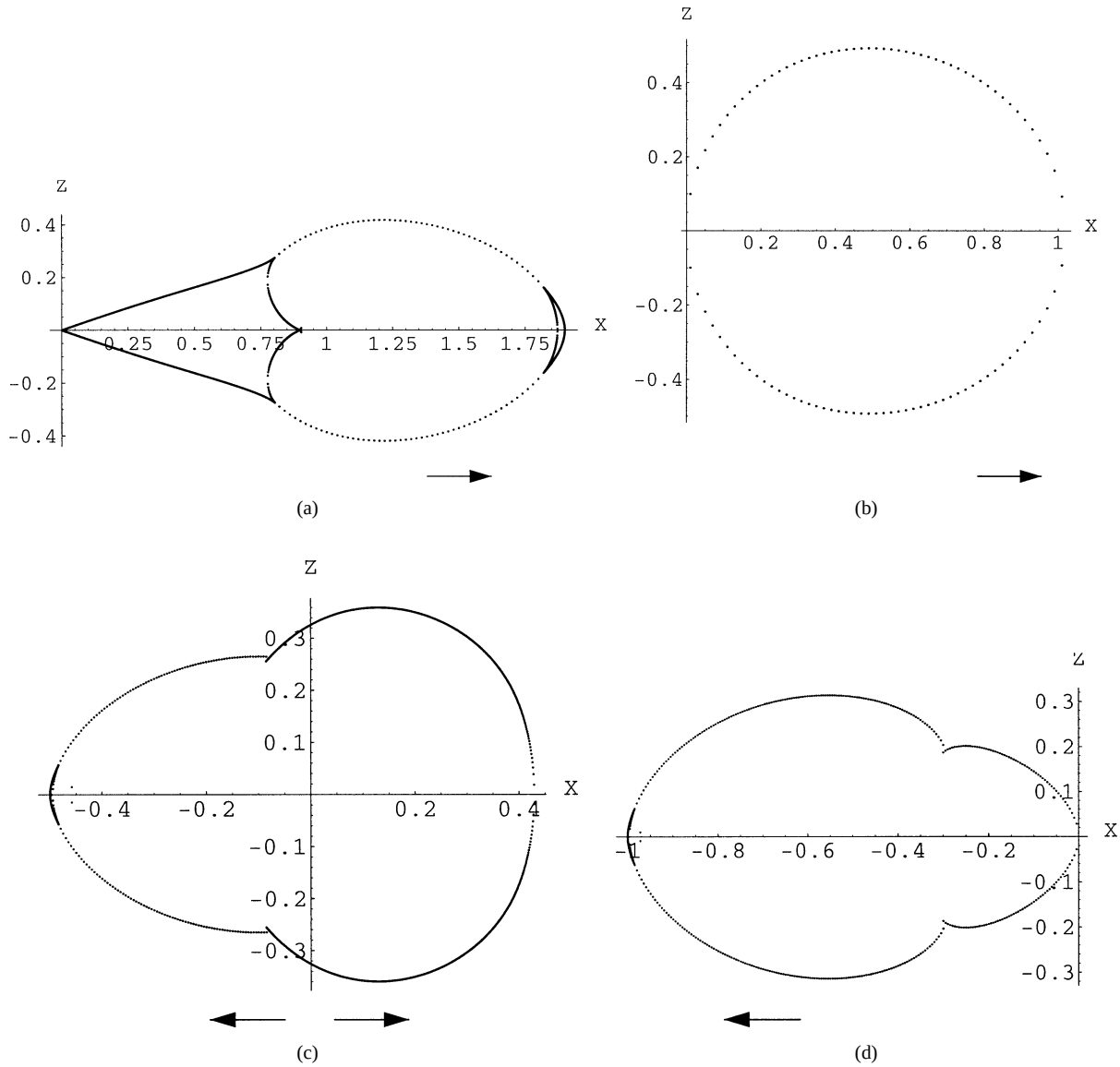

Fig. 7. Spot shapes when $Y = 0.5$. (a) $B = 0.1$ showing the leading and trailing edge oscillatory regions separated by the region in which the perturbations are exponentially large. (b) $B = 1.0$, and the flow is about to reverse. The perturbations increase exponentially inside the whole boundary. (c) $B = 1.5$. The exponentially large perturbations now travel in both X-directions. (d) $B = 2.0$ and the disturbances travel in the negative X-direction only. In (a) the closed curves with heavy lines are obtained as in Fig. 2(b). All other curves are obtained by solving (30) and (63a) with (15), and bound regions of exponentially-growing wall-pressure perturbations.

axis, in contrast to the small adverse pressure-gradient situation of Smith and Timoshin [16] where it moves away from the axis at some distance from the leading edge. At $B = 0.1$, the asymptotic expansion predicts a limiting spot extension of $0 \leqslant X \leqslant 1.9$ and half-width 0.418 as shown in Fig. 7. In the limit $t \to \infty$, decaying oscillatory regions remain in the neighbourhood of the leading and trailing edges, reminiscent of the bow waves observed by Gostelow et al. [8] although, of course, their experiments were for the development of a turbulent spot. The maximum pressure perturbation in Fig. 8 for the case $B = 0.1$ (top left) is $5.9/4\pi^2$ and occurs at about 50% chord. The circular shape of the region of greatest perturbation predicted in Section 5 in the limit $B \to 0^+$ is still evident at this value of B, and is well established at this moderate value of t. When $B = 1$, top right in Fig. 8, the flow is just about to reverse and the profile in Fig. 1 is zero for $0 \leqslant y_1 \leqslant 1$. The limiting spot extension is $0 \leqslant X \leqslant 1$ and has half-width 0.493 as shown in Fig. 7(b). The spot outline itself is almost circular and contains two distinct concentrations of exponentially growing perturbations. The maximum pressure perturbation is $21.52/4\pi^2$ occurring at about 57% chord.

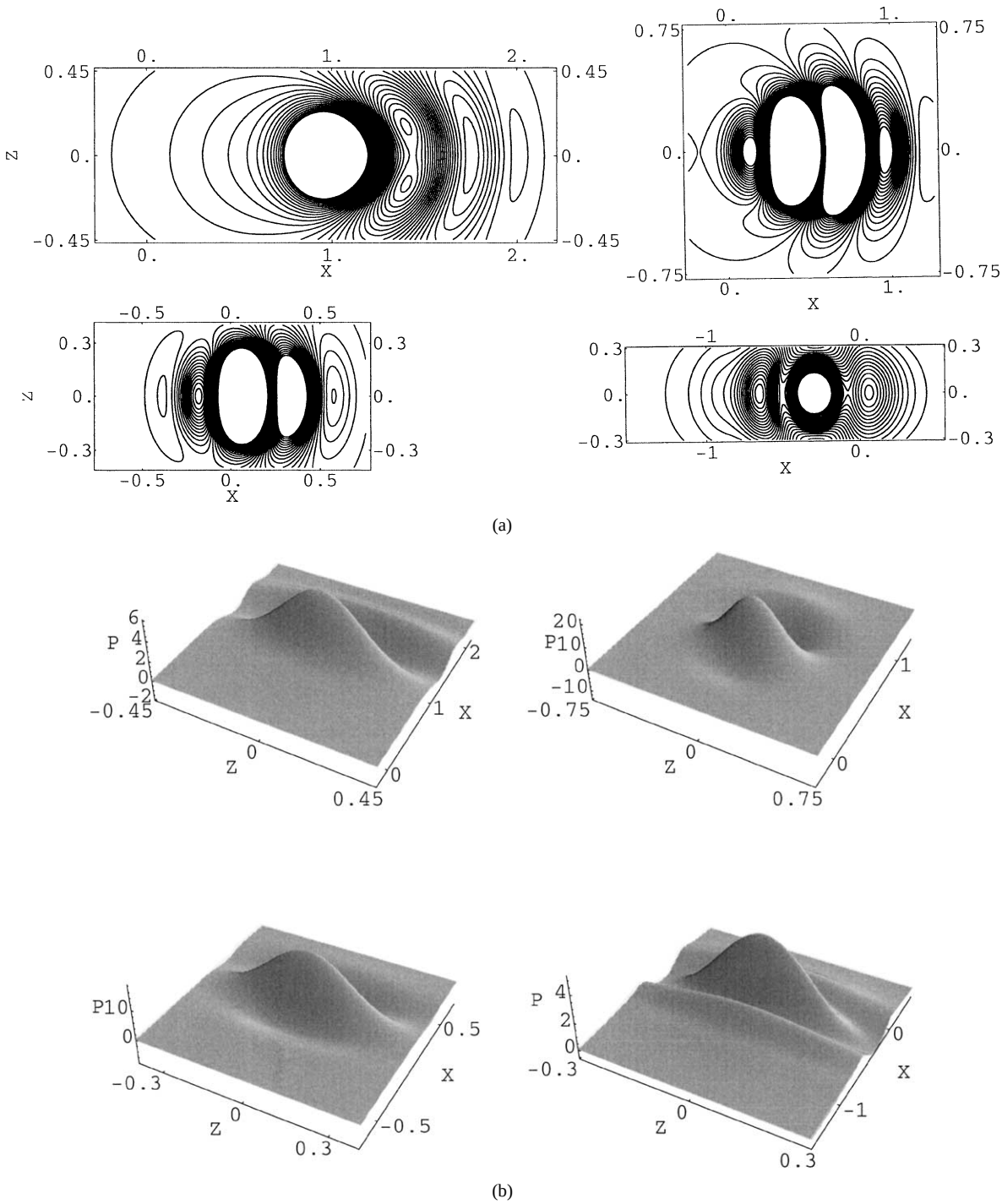

Fig. 8. (a) Wall pressure contours when $t = 20$, $Y = 0.5$ with $B = 0.1$, 1.0 (top row) and $B = 1.5$, 2.0 (bottom row). (b) The corresponding wall pressures (times $4\pi^2$). The spot shapes are shown in Fig. 7.

For $B = 1.5$, lower left in Fig. 8, the perturbations are travelling both upstream and downstream and the spot is expanding in both directions. The limiting extension is $-0.5 \leqslant X \leqslant 0.5$ with maximum half-width 0.359 as in Fig. 7(c). When $t = 20$, as shown here, the maximum value of the perturbation is $17.86/4\pi^2$ at 44% chord. Now the inner part of the boundary layer is fully reversed and the flow is absolutely unstable. In their study of the stability of separation bubbles, Hammond and Redekopp [18]

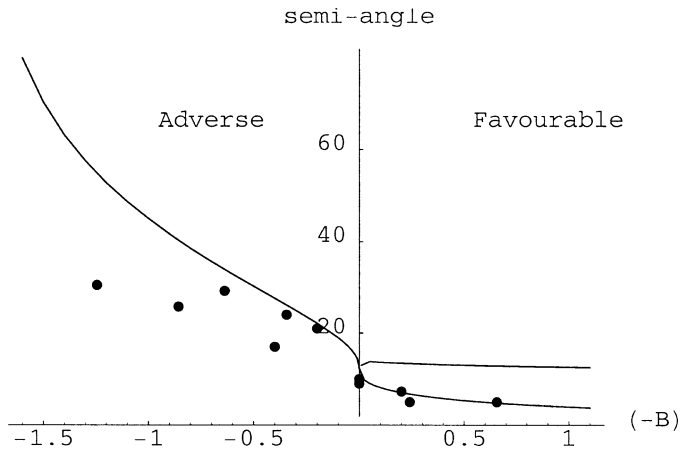

Fig. 9. The spot spreading half-angle in degrees as a function of the pressure gradient parameter $(-B)$ when $Y = 0.5$. Continuous lines—present results. Discrete points—experimental results quoted in [8,10].

have demonstrated the possibility of global instability, and the experimental results of Gostelow and co-workers [8–10] clearly show waves moving both upstream and downstream. The present study supports these predictions.

In Fig. 8, when $B = 2.0$ (lower right) the mainstream itself is about to reverse with the inner part of the flow becoming a jet in what was formerly the upstream direction. Now the perturbations travel upstream only. The limiting extension is $-1 \leqslant X \leqslant 0$ with half-width 0.314 as in Fig. 7(d) and although the entire profile contains exponentially growing perturbations they are not so large; the maximum value is $5.16/4\pi^2$ at about 32% chord. In addition, the circle evident in the lower right contour plot of Fig. 8(a) shows that the features of $B = \infty$ are being approached. In this limit, as explained in Section 3, the BS spot is obtained and indeed it may be shown that, as B decreases from infinity, the BS type spot develops an exponentially growing perturbation in a circular region. The analysis is similar to that of section 5 for $0 < B << 1$, but is not presented here, as it requires either $B \to \infty$ for fixed Y which results in a completely reversed mainstream, or $B \to \infty$ with $Y \to 0$, neither of which cases is strictly relevant to the situation here.

The plot in Fig. 9 is an attempt at an analogue of Fig. 6 of D'Ovidio et al. [10] (see also Fig. 9 of Gostelow et al. [8]). These figures present a compilation of spot-spreading half-angles as a function of pressure gradient parameter. The pressure-gradient parameter λ_θ is related to the parameter in the Falkner–Skan profiles while we have used our parameter B, which is positive for adverse gradients and negative for favourable ones. We have assumed a linear relation between the two parameters with $B = 0$ corresponding to $\lambda_\theta = 0$ and zero pressure gradient, and $B = 1$ to $\lambda_\theta = -0.09$, the laminar separation value proposed by Curle and Skan [19]. This enables the experimental values for the spreading angles quoted in [8,10] to be plotted on our graph. Our ordinate in Fig. 9 is also in degrees and the continuous curve is the angle $\tan^{-1} Z/X$, where Z is the maximum half-width of the spot and X is the position where it occurs. Two curves are shown for $(-B) > 0$ since in this range each portion of the curve has a maximum width (see Fig. 2(b) for example). The lower, decaying curve corresponds to the leading spot, and the higher, almost constant, curve to the trailing spot. For $0 < (-B) < 0.175$ the larger of the maximum widths is attained by the leading spot, and for $(-B) > 0.175$ by the trailing spot (see Fig. 6 where the two widths are equal). When $(-B) = 0.175$, the angle defined by the larger of these maxima jumps discontinuously from the lower to the higher curve. The available experimental values lie well in the lower (leading spot) curve, a possible explanation being that at these values of the pressure gradient the perturbation corresponding to our leading spot is dominant in the experiments. As $(-B) \to \infty$ the trailing spot attains the zero pressure-gradient form of BS and the leading spot disappears. However, in a limited range of B, the results clearly permit qualitative comparison with those of Gostelow et al. At the adverse/favourable divide we have approximately 13° versus experimental values of around 11° while at laminar separation $(-B) = -1$ we predict a rather too large 45° instead of the experimental value of about 30°. There is agreement in the conclusion that the spreading angle increases strongly as adverse pressure gradients become more intense. The superficial comparison is encouraging but of course we are attempting to compare a turbulent experiment with a theoretical study of a perhaps highly idealised laminar flow.

8. Further comments

The linear theory of inviscid three-dimensional disturbances works in the sense that the 'spot' that develops has well-defined boundaries, giving apparently physically sensible spot shapes for the disturbances evolving from an initial-value problem. The

cases of an adverse pressure gradient studied here are distinct from the favourable cases also addressed herein, and the previous case of zero gradient in BS, mainly because the adverse ones yield an exponentially growing response, which mirrors the implicit existence of inflection points in the underlying motion. There is thus a substantial change in character and this shows itself in the different typical spot shapes and spread rates.

Comparisons with experiments are made somewhat tentatively here of course, due to the turbulent nature in most of the experiments and the laminar flow basis in the theory. Nevertheless there are three points of at least qualitative compatibility in pressure-gradient boundary-layer spots which add to the agreements on spread rate and compressibility effects in the zero-gradient case noted in the introduction. The first is on bow waves as described earlier in connection with Fig. 7(a) and observed by Gostelow et al. The second is on the spreading half angle, in Fig. 9 over a wide range of pressure gradient conditions. The third is on Narasimha's [17] experimental findings of a distinct change in the spot spread rate and related characteristics as a boundary layer progresses through a zone of increasingly adverse pressure-gradient. The change is predominantly an abrupt increase in spread rate, helpfully termed a 'subtransition' by Narasimha, and it accords with the present findings. The theory overall provides some support, if not an alternative, to the experimental observations which likewise have large typical Reynolds numbers.

The spot shapes are also of concern. In the favourable-gradient case it would be interesting for the sake of modelling to know whether, for the double spots in Figs. 2–6, each separate spot is related to one of the boundary conditions at the two assumed junctions y_1, y_2, or not. Such spot-splitting however could well be a feature peculiar to the present model with its non-smooth basic velocity profile. Noting that strictly the separate spots are joined together by a connecting line, we could expect a smooth velocity profile to yield a somewhat smoothed-out version of the planforms of Figs. 2–6. Indeed, it would be of interest theoretically to discover not only whether any double spot can occur under a realistic smooth velocity profile in the favourable-gradient case, but also whether an abrupt increase in spread rate is common for adverse pressure-gradients when the basic velocity profile is smooth. The adverse-gradient case is touched on qualitatively in the comparisons of the previous paragraph, but for the favourable-gradient case, our comments earlier in the present paragraph suggest that direct comparisons would be premature with the relatively few experimental or empirical results on actual spot-planform shapes in detail.

Concerning further study, the initiation of the spots is also of interest. Initiation in practice is usually by forcing at the wall or external to the boundary layer as in the wake-passing phenomenon, and Smith and Timoshin [16] show a direct analogy between the two in their context of flow with a near-wall inflection point. It would be interesting to extend that aspect of initiation to the present setting. Likewise of further concern are the influences of nonlinearity, nonparallelism and compressibility. In the case of nonlinearity Smith and Timoshin's study points to an explanation of the calmed region (again see Section 1), which has practical significance for relaminarisation of the flow behind a spot and which would be interesting to pursue in the present context.

Acknowledgements

Comments and interest from Professors Gary Brown, Henrik Alfredsson, Roddam Narasimha, Paul Gostelow and the referees are gratefully acknowledged.

References

[1] G.B. Schubauer, P.S. Klebanoff, Contributions on the mechanics of boundary-layer transition, NACA Rep. 1289 (1955).
[2] I. Wygnanski, M. Zilberman, J.H. Haritonidis, On the spreading of a turbulent spot in the absence of a pressure gradient, J. Fluid Mech. 123 (1982) 69–90.
[3] M. Sankaran, A.J. Chambers, R.A. Antonia, The influence of a favourable pressure gradient on a turbulent spot, in: Proc. 9th Australasian Fluid Mechanics Conference, Auckland, 1994, pp. 342–345.
[4] Y. Katz, A. Seifert, I. Wygnanski, On the evolution of the turbulent spot in a laminar boundary layer with a favourable pressure gradient, J. Fluid Mech. 221 (1990) 1–22.
[5] J.P. Gostelow, G. Hong, N. Melwani, G.J. Walker, Effects of free-stream turbulence and adverse pressure gradients on boundary-layer transition, ASME paper no. 93-GT-377 (1993).
[6] A. Seifert, I. Wygnanski, On turbulent spots in a laminar boundary layer subjected to a self-similar adverse pressure gradient, J. Fluid Mech. 296 (1995) 185–209.
[7] B.F.A. van Hest, D.M. Pesschier, J.L. van Ingen, The development of a turbulent spot in an adverse pressure gradient boundary layer, in: Proc. IUTAM Symposium, Sendai, Japan, 1994.
[8] J.P. Gostelow, N. Melwani, G.J. Walker, Effects of streamwise pressure gradient on turbulent spot development, ASME J. Turbomachinery 118 (1996) 737–743.
[9] A. D'Ovidio, J.A. Harkins, J.P. Gostelow, Turbulent spots in adverse pressure gradients. Part 1. Spot behaviour, ASME paper no. GT-194 (2001).

[10] A. D'Ovidio, J.A. Harkins, J.P. Gostelow, Turbulent spots in adverse pressure gradients. Part 2. Spot propagation and spreading rates, ASME paper no. GT-406 (2001).
[11] D.J. Doorly, F.T. Smith, Initial-value problems for spot disturbances in incompressible or compressible boundary layers, J. Engrg. Math. 26 (1992) 87–106.
[12] J.P. Clark, T.V. Jones, J.E. LaGraff, On the propagation of naturally-occurring turbulent spots, J. Engrg. Math. 28 (1994) 1–19.
[13] R.G.A. Bowles, F.T. Smith, Short-scale effects on model boundary-layer spots, J. Fluid Mech. 295 (1995) 395–407.
[14] S.N. Brown, F.T. Smith, Spot concentrations of large-amplitude disturbances in laminar boundary layers, Quart. J. Mech. Appl. Math. 52 (1999) 269–281.
[15] D.J. Savin, F.T. Smith, T. Allen, Transition of free disturbances in inflectional flow over an isolated surface roughness, Proc. Roy. Soc. A 375 (1999) 491–541.
[16] F.T. Smith, S.N. Timoshin, On spot evolution under an adverse pressure gradient, J. Fluid Mech. 430 (2001) 169–207.
[17] R. Narasimha, Experiments showing subtransitions in spots under an adverse pressure gradient, in: Proc. Workshop (Minnowbrook III) on Turbomachinery Flows, Syracuse, NY, 2000.
[18] D.A. Hammond, L.G. Redekopp, Local and global instability of separation bubbles, European J. Mech. B Fluids 17 (1998) 145–164.
[19] N. Curle, S.W. Skan, Approximate methods for predicting separation properties of laminar boundary layers, Aeronaut. Quart. 8 (1957) 257–268.